

## ORIGINAL ARTICLE

# Characterization of particle dispersion and volume fraction in alumina-filled epoxy nanocomposites using photo-stimulated luminescence spectroscopy

Amanda Stevenson, Ashley Jones and Seetha Raghavan

A novel method is presented to validate the dispersion of  $\alpha$ -alumina nanoparticles within a polymer matrix, as well as to create a calibration for filler particle volume fraction identification. Using photo-stimulated luminescence spectroscopy (PSLS), spectral information from  $\alpha$ -alumina-filled epoxy nanocomposites consisting of varying volume fraction quantities of alumina nanoparticles was collected and analyzed. Surface contour maps of each nanocomposite were created by comparing integrated intensity data from the R1 curve of  $\alpha$ -alumina throughout each specimen. These maps show satisfactory dispersion of alumina in the 5 and 25% volume fraction composites, whereas agglomerations were detected in various regions of the 38% nanocomposite, establishing the capability of this method to characterize photo-luminescent particle dispersion. This new approach also provides high spatial resolution, which can be used to determine the exact locations of voids, inclusions and/or agglomerations, while also predicting the volume percentage of photo-luminescent particle content within a specimen, lending itself as a quality control method in the manufacturing of these composites.

*Polymer Journal* (2011) 43, 923–929; doi:10.1038/pj.2011.82; published online 31 August 2011

**Keywords:** alumina nanocomposites; nanoparticle dispersion; photo-stimulated luminescence spectroscopy

## INTRODUCTION

Thermosetting polymers, such as epoxy resins, are currently being used in aerospace applications because of the ease for which their molecular structure can be modified, as well as their ability to sufficiently bond with various filler materials.<sup>1</sup> Typically, un-reinforced epoxies show poor resistance to crack initiation and propagation.<sup>2</sup> As a result, epoxies are commonly reinforced with filler particles, or modifiers, that alter their molecular structure by increasing the already dense cross-linked network structure of the epoxy, resulting in improved mechanical properties, such as strength, stiffness and toughness.

Recent research has indicated that using nano-sized particles improves the stiffness, strength and toughness of a polymer without sacrificing the thermomechanical properties.<sup>2,3</sup> In addition, nanoparticles have a higher specific surface area than micron-sized particles, as more of these particles can be integrated within a specific volume, enabling an overall increase in the mechanical properties of the matrix.<sup>1,4,5</sup> Commonly embedded nanoparticles include aluminum oxide,<sup>6–8</sup> calcium silicate<sup>6</sup> and titanium oxide.<sup>6,9</sup> With the improvement in mechanical properties, these nanocomposites have applications as ballistic materials with high-impact resistance.<sup>10,11</sup> Owing to a high dielectric strength, alumina-filled epoxy composites are also used in high-voltage applications, such as the encapsulation of ferroelectric elements for shock depoling.<sup>12</sup>

Despite their growing usage, however, the manufacturing process for these materials is complex and the repeatability of the material configuration has limited control. Some of the challenges in the polymer–particle fabrication process include ensuring uniform particle dispersion and accurately controlling the volume fraction or weight percentages of the fillers during manufacturing. For optimized mechanical properties, a homogeneous dispersion of particles must be present, coupled with the non-existence of inclusions, agglomerations or aggregates, as these material flaws can contribute to stress concentrations and lead to premature structure failure. Ensuring that the desired amount of modifier is added to the matrix is also an important aspect of the design process, as this quantity directly affects the mechanical properties of a specimen and determines the cross-link density of the matrix.

Although the primary focus of integrating filler particles into an epoxy resin is improvement of mechanical properties, implementing particles, which are also photo-luminescent can offer additional benefits by exploiting their spectral properties. The spectral properties, as described in this work, provide a means of evaluating particle dispersion and volume fraction percentage within a specimen. One such filler material that offers both of these advantages is aluminum oxide, known as alumina. Previous  $\alpha$ -alumina luminescence applications include the monitoring of pressure in diamond anvil cells,<sup>13</sup> the

determination of stresses in polycrystalline ceramics<sup>14–16</sup> and alumina-filled composites for electronic applications,<sup>17</sup> as well as the integrity assessment of thermally grown oxide of thermal barrier coatings<sup>18–21</sup> on jet engine turbine blades.

Here, a new method is validated, using alumina-epoxy nanocomposites, to verify the homogeneous dispersion of photo-luminescent filler particles and to create a calibration for determining particle content within a polymer matrix. Spectral information was collected from the composites and the integrated intensity parameter was compared to generate contour maps that visually displayed differences in the alumina content throughout the surface. This technique provides surface maps with a high spatial resolution of a few microns, dependent upon both the number of spectral collection points and the objective magnification.

### Spectral relationships

The spectral properties of alumina have been previously exploited for their ability to evaluate the stress of a material. Using a method known as piezospectroscopy, stress-induced shifts of the characteristic R-lines present in the emission spectrum of chromium-doped alumina can be directly correlated to stress. Although piezospectroscopy specifically uses the peak positions of the R-lines for stress measurement, photo-stimulated luminescence spectroscopy (PSLS), in general, can measure other spectral properties such as the integrated intensity of the R-line curves, studied here for its capability to assess the dispersion and volume fraction of particles. This characteristic is defined as the area under each R-line curve and is a direct measure of the energy emitted from the chromium ions that reside within the alumina lattice, shown in Figure 1. As these chromium ions are excited by an external source such as a laser, they release photons because of the transition from higher energy levels back to ground state. The emitted photon energy can be quantified using the following equation:

$$E = h\nu \quad (1)$$

where  $E$  is the energy of the photon (J),  $h$  is Planck's constant ( $6.63 \times 10^{-34}$  Js), and  $\nu$  is frequency (Hz or  $s^{-1}$ ).

## EXPERIMENTAL PROCEDURE

### Materials

The photo-luminescent filler material used in this work was  $\alpha$ -alumina nanoparticles having an average crystal size of 40 nm and an average particle size of 150 nm. Transmission electron microscopy images were captured to validate particle size and geometry, as seen in Figure 2. The alumina particles and aggregates were determined to have size distributions ranging from approximately 50 to 500 nm, having amorphous configurations. These particles

were of 99.85% purity, providing sufficient chromium-content within the alumina. Owing to low room temperature viscosity, long working life and low moisture absorption, Epon 862 and Epikure W were selected as the resin-curing system.

### Fabrication and manufacturing of alumina-filled epoxy nanocomposites

Three different alumina-epoxy nanocomposites were manufactured consisting of 5, 25 and 38% alumina by volume. This range was established based on literature indicating that a minimum of 5% volume fraction has a positive influence on mechanical properties,<sup>22</sup> and 43% has been determined to be the maximum amount of alumina that can be added conveniently to an epoxy, using standard manufacturing methods, without having a negative effect on the overall properties of the epoxy.<sup>5</sup> The manufacturing procedure was based on literature describing the addition of alumina fillers in epoxy composites for mechanical property improvements.<sup>11,23–25</sup> For each volume fraction composite fabrication, the epoxy resin, curing agent and  $\alpha$ -alumina particles were initially mixed using a high-shear mixer for the duration of 15 min to break up any agglomerates present, while also dispersing the alumina homogeneously within the epoxy. Once combined, the material was placed into a sonicator for  $\sim 20$  min to further ensure homogeneity, as well as cause any entrapped air bubbles to surface for removal. The composite was then placed inside a low-pressure desiccator–vacuum system for  $\sim 45$  min or until no air bubbles were visible and subsequently transferred and poured into an aluminum mold with the dimensions  $10 \times 6 \times 3.5$  inch, which was first prepared with a mold release. A two-step curing process with duration of 6 h at  $54^\circ\text{C}$  and 16 h at  $93^\circ\text{C}$  was implemented and the specimens were allowed to cool.

The alumina-filled epoxy nanocomposites were cut from the aforementioned bulk samples. Three samples of each volume fraction were manufactured

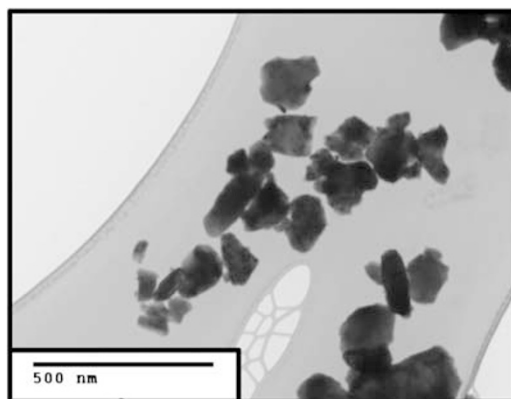


**Figure 2** Transmission electron microscopy image showing the overall shape and size of the  $\alpha$ -alumina nanoparticles.

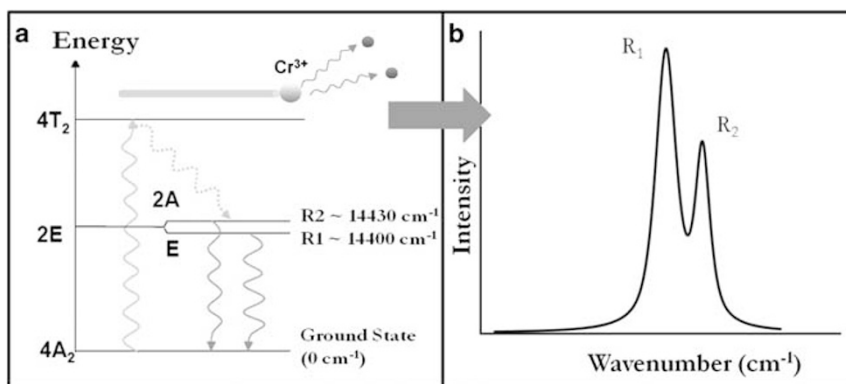


**Figure 1** (a) Energy emitted from chromium-doped alumina resulting in (b) the R-lines of  $\alpha$ -alumina. A full color version of this figure is available at *Polymer Journal* online.



**Figure 3** Images showing the size of the nanocomposites (a) as compared with a dime and (b) measured with a ruler. The final dimensions of the  $\alpha$ -alumina nanocomposites were  $1/8 \times 1/8 \times 1/2$  inch. A full color version of this figure is available at *Polymer Journal* online.

into parallelepipeds having a 4:1 ratio per ASTM D695 in preparation for mechanical testing. The ratio was chosen to avoid edge effects caused by the friction between the sample surface and the platen during loading experiments, which were previously observed in *ex-situ* studies of compression tests on polycrystalline alumina of a lower aspect ratio.<sup>26</sup> The calibration of PSLs peak shifts in these separate compression tests of the specimens are reported elsewhere.<sup>27</sup> The final dimensions of the samples included a  $1/8 \times 1/8$ -inch cross-section and a length of  $1/2$  inch, shown in Figure 3.

### PSLS measurements

To create the high spatial resolution spectral surface mappings, a unique system consisting of an MTS Insight electromechanical testing system (MTS System Corporation, Eden Prairie, MN, USA), fiber optic probe, xyz stage and Raman spectrometer was used to collect luminescence data and is shown in Figure 4.<sup>28</sup> The Raman spectrometer was coupled with a green, argon laser, which operated at a wavelength of 532 nm and exerted a maximum output power of 50 mW. The laser beam had the capability of either being directed to an attached microscope or to a connecting fiber optic probe. The fiber optic probe was coupled with the Raman system via optical cables and an objective lens of  $\times 10$  magnification was used based on the ideal focal distance for our experimental setup. A special mount to hold the probe stationary was created and attached to the y axis of the xyz stage, whereas the xyz stage itself was fastened to a platform that was built and affixed to the base of the MTS machine. The laser dot was initially focused on the specimen by incrementally moving the probe in the z direction (toward or away from the sample), while simultaneously collecting spectral data. The optimal focal distance was achieved when the intensity of the R1 peak was observed at a maximum value. This focus distance was kept constant for all data collection areas on that specimen surface. There were a total of 100 data collection regions per sample surface; 5 points in the x direction and 20 points in the y direction. The fiber optic probe was set to collect data in the upper left-hand corner of each surface at the beginning of each mapping and luminescence data from each region was collected in a 'snake scan' pattern, as seen in Figure 5.

### Deconvolution and curve fitting of spectral data

Owing to their close proximity to each other, the R-lines produced from  $\alpha$ -alumina overlap and share information. Therefore, to properly analyze the spectral characteristics collected from the alumina nanocomposites, the raw, experimental data was processed using a deconvolution and fitting program, as shown in Figure 6. Throughout this work, a genetic algorithm-based procedure previously created and used to predict the correct R-line and vibronic sideband peak positions of polycrystalline alumina<sup>29</sup> was implemented on the unprocessed, experimental data. This Matlab-based, genetic algorithm method was preferred over gradient-based methods, as it has the capability of global optimization<sup>30,31</sup> and performs four main functions to optimize the R-lines: baseline removal, cropping, separation and recombination. The fitting procedure used two pseudo-Voigt functions<sup>32-34</sup> to obtain the following design variables for each of the R1 and R2 curves: area, line-widths, peak positions and shape factors (describing the Gaussian and Lorentzian characteristics).<sup>35</sup>

## RESULTS AND DISCUSSION

### Integrated intensity maps: particle dispersion verification

The capability of detecting and measuring the R-lines from  $\alpha$ -alumina nanoparticles embedded within an epoxy resin was determined and

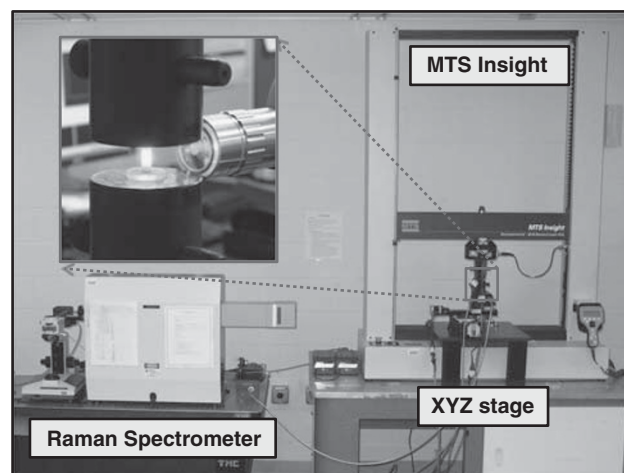


**Figure 4** Unique experimental system used to create spectral contour maps integrated with a Raman spectrometer, xyz stage and MTS Insight machine. A full color version of this figure is available at *Polymer Journal* online.

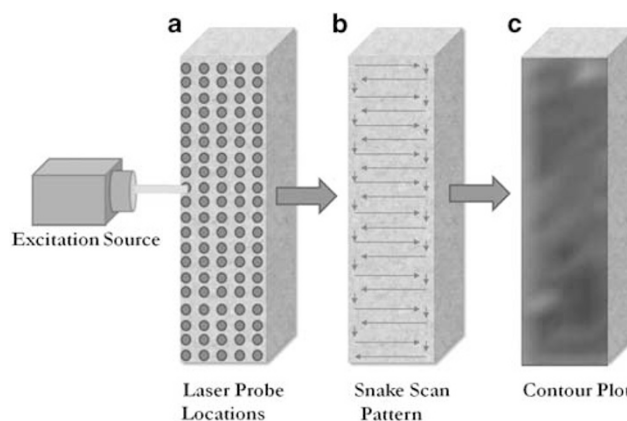


**Figure 5** Schematic showing data collection at (a) laser-probe locations in a (b) snake scan pattern where data collected is illustrated as (c) an integrated intensity contour plot. A full color version of this figure is available at *Polymer Journal* online.

verified in this work. Photo-stimulated luminescence readings from all three  $\alpha$ -alumina-epoxy nanocomposites were obtained as shown in Figure 7, showing strong intensities from the 25 and 38% samples. In addition, a comparison of R-lines from polycrystalline alumina and those obtained from the 38% alumina nanocomposite shows that the overall line shape distribution between the two materials is similar, as presented in Figure 8.

As previously described in the Experimental procedure section, independent luminescence measurements were collected from each of

the 100 target areas per sample surface. Four spectral parameters of the R-lines were exploited from the data: peak position, Gaussian distribution, intensity and integrated intensity. A comparison between the integrated intensities from each volume fraction nanocomposite is presented in Figure 7, indicating an evident correlation between integrated intensity and  $\alpha$ -alumina particle content. It was observed that an increase in particle volume fraction was accompanied by an increase in the magnitude of the emission intensity. As the concentration of  $\alpha$ -alumina increases, the probability of the incident beam interacting with a nanoparticle also increases and is governed by the following equation:

$$P = N\sigma \quad (2)$$

where  $P$  is the interaction probability,  $N$  is the number of atoms or ions and  $\sigma$  is the microscopic cross-section.

Thus, the overall energy emitted from an  $\alpha$ -alumina composite is directly related to the amount of photo-luminescent particles present. With this relationship, the homogeneity and/or alumina content throughout a specimen can be determined.

Spectral contour maps comparing the integrated intensity throughout the surface of each nanocomposite is shown in Figure 9. Using the relationship between particle content and intensity magnitude, a contour map exhibiting a monochromatic color scheme indicates a homogeneous distribution of  $\alpha$ -alumina nanoparticles. Regions exhibiting higher intensity magnitudes as compared with other locations on the specimen indicate the presence of more  $\alpha$ -alumina particles within that localized volume, whereas areas with comparatively low-intensity values suggest an absence of particles. The high spatial resolution results indicate large variations in the 5% specimen,

whereas the 25% and 38% specimens displayed slightly smaller intensity distributions. As there are less alumina particles residing in the 5%, we would expect there to be regions lacking in particle content, which would present itself as large-intensity variations as compared with areas having particles. The distribution of alumina within the 25 and 38% nanocomposites show deviations in intensity as well, where the darker regions indicate the presence of more particles.

In order to provide an initial assessment of nanoparticle dispersion in the manufactured samples for PLS measurements, scanning emission microscopy images were taken for each of the samples and shown in Figure 10. Using a Hitachi S3500N system (Hitachi Ltd., Tokyo, Japan), operated at 20 kV, back scattering from aluminum was collected to display particle dispersion. The aluminum (contained within the alumina nanopowder) appears darker than the K- $\alpha$  X-rays, which are represented by the white regions. Therefore, from the small collection region illustrated in the images, it was shown that for all volume fractions, there is a sufficient homogenous distribution of the particles and the samples were suitable for further PLS studies.

The use of PLS to assess particle distribution not only offers an alternative method to scanning emission microscopy imaging for dispersion studies but is also non-invasive and provides high spatial resolution measurements over a larger surface area of measurement. Furthermore, the need for surface or sample preparation, which can create surface damage or result in a decrease in the mechanical properties of a specimen, is not required to obtain photo-luminescence measurements. Ultimately, these spectral-integrated intensity contour maps using PLS significantly enhances the ability to assess the distribution of particles achieved in the manufacturing of these

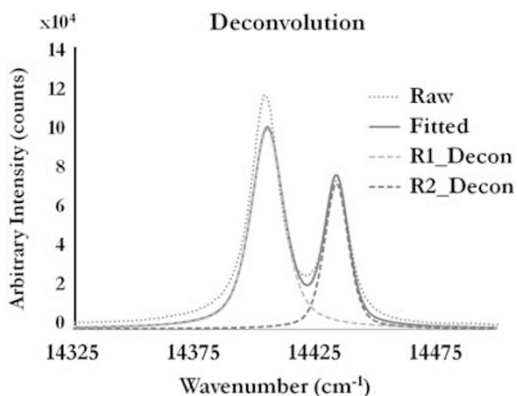


**Figure 6** Deconvolution and curve-fitting process for the R-lines of  $\alpha$ -alumina. A full color version of this figure is available at *Polymer Journal* online.

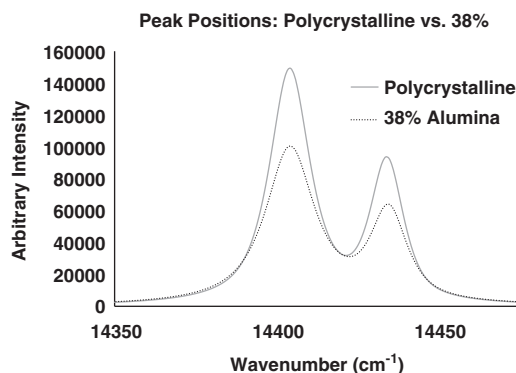


**Figure 8** Comparison of R-line shape and distribution of the 38% nanocomposite to polycrystalline alumina. A full color version of this figure is available at *Polymer Journal* online.

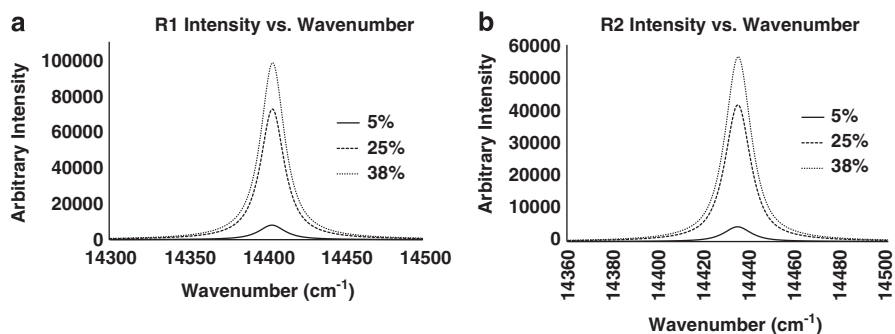


**Figure 7** Intensities obtained from 5, 25 and 38% volume fraction  $\alpha$ -alumina nanocomposites for (a) R1 and (b) R2. A relationship between intensity and particle quantity is presented.

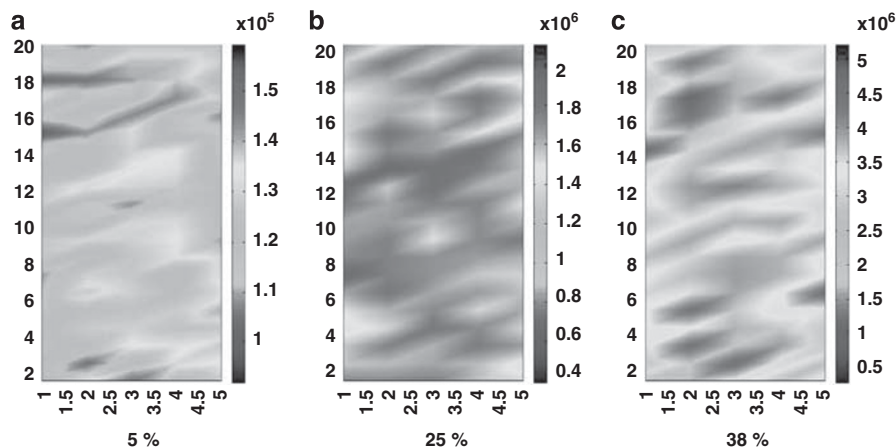


**Figure 9** Local contour plots for the intensity of (a) 5, (b) 25 and (c) 38% volume fraction  $\alpha$ -alumina nanocomposites illustrating individually the small variations in dispersion within each sample. Note that the corresponding scale is different for each sample and represents the minimum and maximum intensity for that sample. A full color version of this figure is available at *Polymer Journal* online.

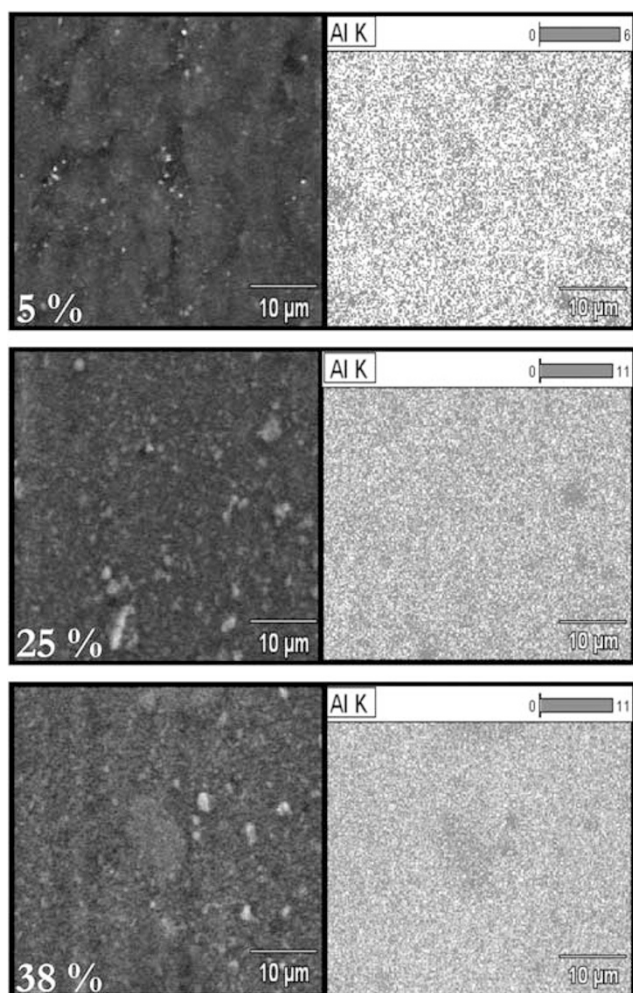


**Figure 10** Scanning emission microscopy imaging verifying the alumina particle dispersion of the 5, 25 and 38% volume fraction nanocomposites. A full color version of this figure is available at *Polymer Journal* online.

nanocomposites, which is often assumed to be represented by localized microscopy measurements. Here, the benefit lies in the capability of this method to display a comprehensive particle distribution

throughout the entire sample, with an accuracy of a few microns in spatial resolution.

#### Quantification of particle volume fraction using integrated intensity

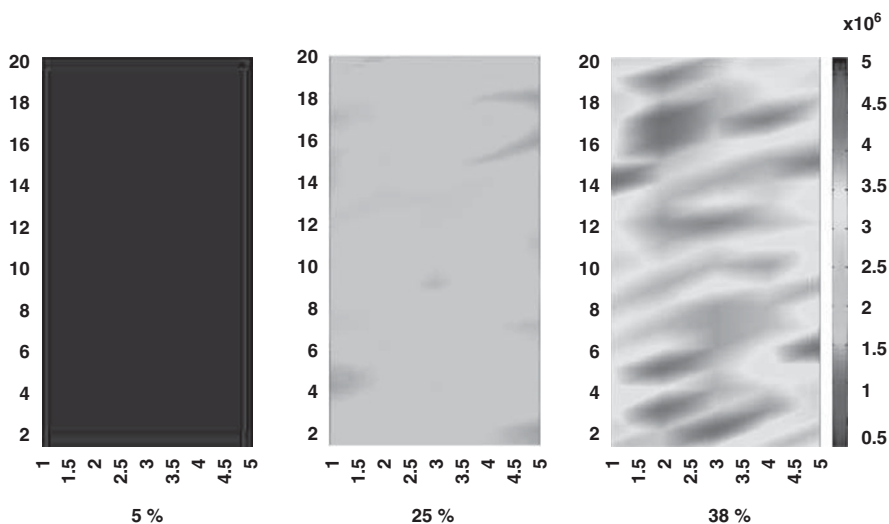
Another important application for contour surface mapping using PLS is the capability of determining the filler particle volume percent of a particular sample. Spectral contour maps were designed to compare the intensity of all three nanocomposites via one scale, using the global maximum and minimum values from all specimens. Comparison of intensity magnitudes on the same scale allows for the determination of particle content. A specimen containing a low quantity of particles would have a relative low-intensity magnitude as compared with a specimen with an increased number of particles. From Figure 11, it is shown that the 5% specimen has intensity values at the lower end of the scale, the intensities for the 25% appear in the middle region, and the 38% has intensities at the top (peak) of the scale. These results were as expected and can provide a calibration system for the determination of particle content within specimens.

Figure 12 shows the calibration of alumina volume fraction with the corresponding integrated intensity values. This relationship can be explained by applying Beer's law to describe the behavior of the collected luminescence due to the interaction between the excitation source and the matrix. By incorporating Beer's law, the luminescence of each nanocomposite can be analyzed, predicting that there exists a relationship between absorbance (and therefore emittance) and the concentration of the material, as described by the following equation:

$$A = -\log T = -\log(\Phi/\Phi_a) = abc \quad (3)$$

where  $A$  is the absorbance of the material,  $T$  is the transmittance,  $a$  is the absorptivity,  $b$  is the path length of the absorption and  $c$  is the concentration of the material that has the absorption properties.

The nanocomposites configured in this study consisted of epoxy resin and  $\alpha$ -alumina nanoparticles. Only the chromium within the alumina exhibited luminescent properties measured here. Therefore, the measured luminescence from the specimens only describes the behavior of the chromium-doped alumina particles. It can be stated that the radiant power that is luminesced is proportional to the



**Figure 11** Global contour plots for the intensity of 5, 25 and 38% volume fraction  $\alpha$ -alumina nanocomposites where the scale represents the minimum and maximum intensity for all volume fractions. A full color version of this figure is available at *Polymer Journal* online.

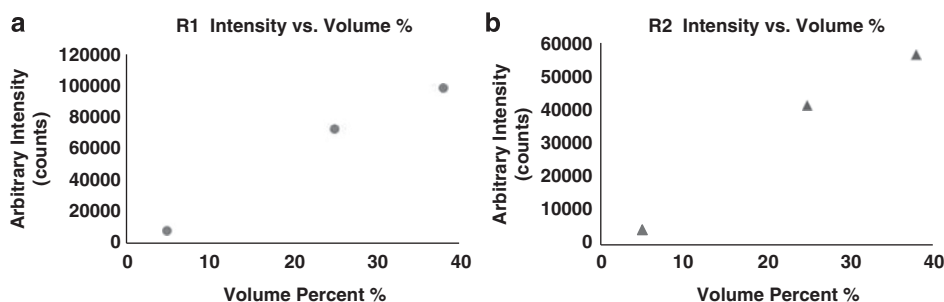


**Figure 12** Increasing integrated intensity values are seen with higher alumina content for (a) R1 and (b) R2. A full color version of this figure is available at *Polymer Journal* online.

amount of power that is absorbed,

$$\Phi_L = k(\Phi_0 - \Phi) \quad (4)$$

where  $\phi_0$  is the radiant power of the incident beam,  $\phi$  is the total power transmitted and  $k$  describes the efficiency at which an excited atom or molecule emits a photon when returning to ground state and varies by material.

Assuming that the transmitted radiant power is equal to

$$\Phi = k\Phi_0 10^{-abc} \quad (5)$$

and combining Beer's law with equation (4), the total power transmitted from a photo-luminescent material is provided as:

$$\Phi_L = k\Phi_0(1 - 10^{-abc}) \quad (6)$$

However, the ability to capture the photo-luminescence of these nanoparticles is altered once embedded within a material of specified density. Although the photo-luminescent behavior of the chromium atoms is still governed by equation (4), the number of photons collected may be less than the actual number of photons emitted, due to absorbance and scattering that occurs within the material itself. Photons capable of being collected by a charged coupling device, exit the specimen in a direction parallel and opposite to the incident beam. Scattered photons will exit in various directions and are, therefore, unaccounted for in the measurement. In addition, an emitted photon

may also be absorbed by a material, prohibiting the energy from escaping. Our results in Figure 12 show a calibration for three different known volume fraction nanocomposites, which represent the relationship between the integrated intensity and the concentration. This trend, as described by Beer's law, follows the expected trend of increasing integrated intensity with concentration and has also been observed in studies of sintered alumina of varying densities.<sup>36</sup> The integrated intensity calibration, which uses known volume fraction  $\alpha$ -alumina-epoxy specimens can be refined to include additional volume fraction specimens. Ultimately, this calibration could be used to identify the amount of nanoparticles contained within unknown volume fraction specimens.

## CONCLUSION

In this work, a novel method to verify the particle dispersion and volume fraction in alumina-epoxy nanocomposites using PLS was presented. Exploiting the spectral properties of  $\alpha$ -alumina nanoparticles, the integrated intensity parameter was used to create contour plots that provided an overall particle distribution within alumina nanocomposites of varying alumina quantity. Verifiable through localized scanning emission microscopy and transmission electron microscopy imaging, the PLS technique provides the ability to map larger surface areas non-destructively, which is especially applicable to thin films, such as adhesives or coatings. Given the aptitude to verify particle dispersion and volume fraction quantities, the application of

this method as a quality control technique can greatly improve the manufacturing of these nanocomposites and, therefore, ensure optimal properties are achieved in applications in which the addition of nanoparticles to an epoxy or polymer are used to improve the mechanical properties. Ultimately, the PLS technique for particle dispersion verification and volume fraction identification can facilitate optimized manufacturing processes, thereby, limiting stress concentrations and ensuring that the most advantageous mechanical properties within the material are achieved.

## ACKNOWLEDGEMENTS

This research was funded by the University of Central Florida Office of Research and Commercialization Inhouse Research Grant FY 2010.

- Zunjarrao, S. C. & Singh, R. P. Characterization of the fracture behavior of epoxy reinforced with nanometer and micrometer sized aluminum particles. *Compos. Sci. Technol.* **66**, 2296–2305 (2006).
- Shukla, D. K. & Parameswaran, V. Epoxy composites with 200nm thick alumina platelets as reinforcements. *J. Mater. Sci.* **42**, 5964–5972 (2007).
- Ahmad, K. & Pan, W. Hybrid nanocomposites: a new route towards tougher alumina ceramics. *Compos. Sci. Technol.* **68**, 1321–1327 (2008).
- Njuguna, J., Pielichowski, K. & Alcock, J. R. Epoxy-based fibre reinforced nanocomposites. *Adv. Eng. Mater.* **10** (2007).
- Gilbert, E. N., Hayes, B. S. & Seferis, J. C. Nano-alumina modified epoxy based film adhesives. *Poly. Eng. Sci.* **43** No 5, 1096–1104 (2003).
- Wetzel, B., Rosso, P., Hauptert, F. & Friedrich, K. Epoxy nanocomposites—fracture and toughening mechanisms. *Eng. Fract. Mech.* **73**, 2375–2398 (2006).
- McGrath, L. M., Parnas, R. S., King, S. H., Schroeder, J. L., Fischer, D. A. & Lenhart, J. L. Investigation of the thermal, mechanical, and fracture properties of alumina-epoxy composites. *Polymer* **49**, 999–1014 (2008).
- Zhao, S., Schadler, L. S., Hillborg, H. & Auletta, T. Improvements and mechanisms of fracture and fatigue properties of well-dispersed alumina/epoxy nanocomposites. *Compos. Sci. Technol.* **68**, 2976–2982 (2008).
- Evora, V. M. F., Jain, N. & Shukla, A. Stress intensity factors and crack velocity relationships for polyester/TiO<sub>2</sub> nanocomposite. *Exp. Mech.* **45**, 153–159 (2005).
- Millett, J. C. F., Bourne, N. K. & Deas, D. The equation of state of two alumina-filled epoxy resins. *J. Phys. D: Appl. Phys.* **38**, 930–934 (2005).
- Song, B., Chen, W., Montgomery, S. T. & Forrestal, M. J. Mechanical response of an alumina-filled epoxy at various strain rates. *J. Compos. Mater.* **43**, 1519–1536 (2009).
- Mock, Jr.W. & Holt, W. H. Shock-wave compression of an alumina-filled epoxy in the low gigapascal stress range. *J. Appl. Phys.* **49** (3), 1156–1158 (1978).
- Barnett, J. D., Block, S. & Piermarini, G. J. An optical fluorescence system for quantitative pressure measurement in the diamond anvil cell. *Rev. Sci. Instrum.* **44**, 1–9 (1973).
- Ma, Q. & Clarke, D. R. Piezospectroscopic determination of residual stresses in polycrystalline alumina. *J. Am. Ceram. Soc.* **77**, 298–302 (1994).
- Raghavan, S. & Imbrie, P. K. Ex-situ stress measurements in polycrystalline ceramics using photo-stimulated luminescence spectroscopy and high-energy x-rays. *Am. Ceram. Soc.* **11** no 11, 1–7 (2009).
- Clarke, D. R. & Gardiner, D. J. Recent advances in piezospectroscopy. *Int. J. Mater. Res.* **98**, 8 (2007).
- Muraki, N., Matoba, N., Hirano, T. & Yoshikawa, M. Determination of thermal stress distribution in a model microelectronic device encapsulated with alumina filled epoxy resin using fluorescence spectroscopy. *Polymer* **43**, 1277–1285 (2002).
- Nychka, J. A. & Clarke, D. R. Damage quantification in TBCs by photo-stimulated luminescence spectroscopy. *Surf. Coat. Technol.* **146–147**, 110–116 (2001).
- Gell, M., Sridharan, S. & Wen, M. Photoluminescence piezospectroscopy a multi-purpose quality control and NDI technique for thermal barrier coatings. *Int. J. Appl. Ceram. Technol.* **1**, 316–329 (2004).
- Raghavan, S. & Imbrie, P. K. The development of photo-stimulated luminescence spectroscopy for 3D stress measurements in the thermally grown oxide layer of thermal barrier coatings. *Proc. Mater. Sci. Technol.* 2056–2067 (2007).
- Sridharan, S., Xie, L., Jordan, E. H. & Gell, M. Stress variation with thermal cycling in the thermally grown oxide of an EB-PVD thermal barrier coating. *Surf. Coat. Technol.* **179**, 286–296 (2004).
- Lee, D. G., Kim, J. K. & Cho, D. H. Effects of adhesive fillers on the strength of tubular single lap adhesive joints. *J. Adhes. Sci. Technol.* **13**, 1343–1360 (1999).
- Setchell, R. E., Anderson, M. U. & Montgomery, S. T. Compositional effects on the shock-compression response of alumina-filled epoxy. *J. Appl. Phys.* **101**, 083527 (2007).
- Lee, M. Y., Ahn, S. K. & Montgomery, S. T. Statistical analysis of compositional factors affecting the compressive strength of alumina-loaded epoxy. *Tech Rep SANDIA National Laboratory SAND2006-0513*, 1–36 (2006).
- Millett, J. C. F., Deas, D., Bourne, N. K. & Montgomery, S. T. The deviatoric response of an alumina filled epoxy composite during shock loading. *J. Appl. Phys.* **102**, 063518 (1–6) (2007).
- PeterImbrie, S. R. High resolution stress mapping of polycrystalline alumina compression using synchrotron radiation. *J. Synch. Rad.* **18**, 497–505 (2011).
- Stevenson, A Calibration of alumina-epoxy nanocomposites using piezospectroscopy for the development of stress-sensing adhesives, University of Central Florida, Florida, (2011).
- Freihofer, G., Poliah, L., Walker, K., Medina, A. & Raghavan, S. Optical stress probe: *in situ* stress mapping with Raman and photo-stimulated luminescence spectroscopy. *J. Instrum.* **5**, P12003 (2010).
- Raghavan, S., Imbrie, P. K. & Crossley, W. A. The spectral analysis of R lines and vibronic sidebands in the emission spectrum of ruby using genetic algorithms. *Appl. Spectro.* **62**, 759–765 (2008).
- Williams, E. A. & Crossley, W. A. Empirically derived population size and mutation rate guidelines for a genetic algorithm with uniform crossover. In *Soft Computing in Engineering Design and Manufacturing*. (Chawdhry P, Roy R, Pant R, eds) 163–172 (Springer-Verlag, London, 1998).
- Crossley, W. & Williams, E. A study of adaptive penalty functions for constrained genetic algorithm-based optimization. *AIAA 35th Aerospace Sciences Meeting and Exhibit*, Reno, Nevada, January 1997. AIAA Paper 97-0083
- Kielkopf, J. F. New approximation to the voigt function with applications to spectral-line profile analysis. *J. Opt. Soc. Am.* **63**, 987–995 (1973).
- Wertheim, G. K., Butler, M. A., West, K. W. & Buchanan, D. N. E. Determination of the gaussian and lorentzian content of experimental line shapes. *Rev. Sci. Instrum.* **45**, 1369–1371 (1974).
- Ida, T., Ando, M. & Toraya, H. Extended pseudo voigt function for approximating the voigt profile. *J. Appl. Crystallogr.* **33**, 1311–1316 (2000).
- Selcuk, A. & Atkinson, A. Analysis of the Cr<sup>3+</sup> luminescence spectra from thermally grown oxide in thermal barrier coatings. *Mater. Sci. Eng.* **AA335**, 147–156 (2002).
- Jankowiak, R., Roberts, K., Tomasiak, P., Sikora, M., Small, G. J. & Schilling, C. H. Probing the crystalline environment of  $\alpha$ -alumina via luminescence of metal ion impurities: an optical method of ceramic flaw detection. *Mater. Sci. Eng.* **AA281**, 45–55 (2000).